Formation and Stability of Synaptic Receptor Domains: Supplemental Material

Christoph A. Haselwandter, Martino Calamai, Mehran Kardar, Antoine Triller, and Rava Azeredo da Silveira

A summary of experimental materials and methods is presented in Sec. S1. Section S2 provides supplementary information on Eqs. (1) and (2) of the main text, and Sec. S3 discusses in greater detail our reaction kinetics for the formation and stability of synaptic receptor domains. Finally, Secs. S4 and S5 provide supplementary information pertaining to the simulations of the steady-state and plasticity of synaptic receptor domains.

S1 Experimental materials and methods

As illustrated in Fig. S1, our minimal experimental system allows for interactions between glycine receptors and gephyrin scaffold proteins, and the diffusion of these molecules at the cell membrane. The construction of the chimeric cDNA for the GlyRα1 subunit bearing the gephyrin binding sequence (βgb) and of the venus-tagged gephyrin (VeGe) have been described earlier [1]. Subconfluent African green monkey kidney (COS-7) cells were co-transfected (FuGENE 6, Roche Applied Science, France) using a total of 2μg plasmid DNA at a GlyR gephyrin stoichiometry of 2:1. At successive times [as indicated in Fig. 1(c) of the main text], GlyR immunolabelling was carried out with primary antibody and secondary antibody coupled to Cy3 (as described previously for the visualization of cell surface receptors [2]), and VeGe fluorescence was visualized directly. The area of GlyR-Vege clusters was quantified using a multidimensional image analysis as described previously [3]. Figure S2 shows the resulting cumulative probability distributions of RSD area for the time points in Fig. 1 of the main text, and provides further evidence for a stable characteristic size of RSDs in our model system.

S2 Reaction-diffusion equations and linear stability analysis

The contributions to the temporal evolution of r and s in Eqs. (1) and (2) of the main text resulting from the diffusion of receptors and scaffolds can be written as the divergence of a current:

$$\left[\frac{\partial r}{\partial t}\right]_{\text{diff}} = -\nabla \cdot \mathbf{j} \equiv -\nabla \cdot (\mathbf{j}_1 + \mathbf{j}_2) \,, \tag{S1}$$

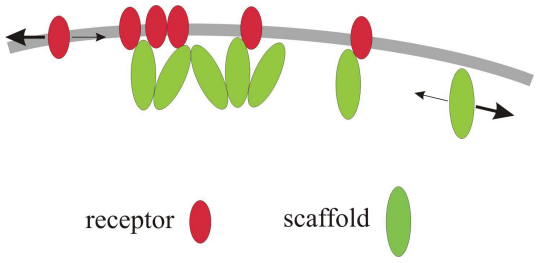

Figure S1: Schematic view of glycine receptors (red) and gephyrin scaffold proteins (green). Both molecular species can diffuse (arrows) and binding can exist between glycine receptors and gephyrin and between gephyrin and gephyrin. Collectively, glycine receptors and gephyrin scaffolds can form domains.

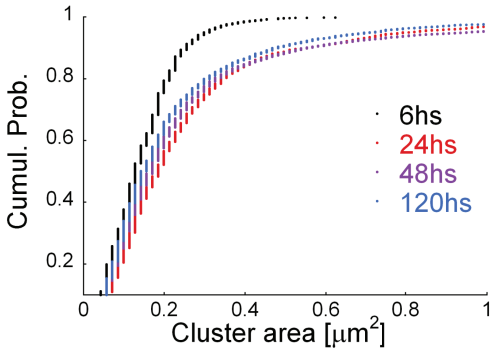

Figure S2: Cumulative probability distribution of cluster (domain) area of RSDs obtained from our experiments for the time points in Fig. 1 of the main text.

where we use the convention that the positive orientations of the current vectors point towards increasing values of x and y. The current

$$\mathbf{j}_1 = -\nu_r(1-s)\nabla r \tag{S2}$$

is in the direction of decreasing r and represents standard surface diffusion in the presence of the excluded-volume species s. The current

$$\mathbf{j}_2 = -\nu_r r \nabla s \tag{S3}$$

is in the direction in which s is decreasing and arises because, due to the exclusion condition, it is favorable for receptor molecules to diffuse into regions with fewer scaffold molecules. Analogous considerations apply to the diffusion of scaffolds. Thus, the nonlinear corrections to the standard diffusion terms $\nu_r\nabla^2 r$ and $\nu_s\nabla^2 s$ describe the effects of steric repulsion of receptors and scaffolds on the diffusion of these molecular species along the cell membrane.

For our model to allow a Turing instability [4–8], Eqs. (1) and (2) of the main text must exhibit a non-trivial homogeneous fixed point $(r,s) = (\bar{r},\bar{s})$ with $\bar{r} \neq 0,1$ and $\bar{s} \neq 0,1$:

$$F(\bar{r},\bar{s}) = 0\,, \qquad G(\bar{r},\bar{s}) = 0\,. \tag{S4}$$

The homogeneous stability matrix for this problem reads

$$\mathbf{M} = \begin{pmatrix} r_{11} & r_{12} \\ s_{21} & s_{22} \end{pmatrix} \equiv \begin{pmatrix} \frac{\partial F}{\partial r}\Big|_{(r,s)=(\bar{r},\bar{s})} & \frac{\partial F}{\partial s}\Big|_{(r,s)=(\bar{r},\bar{s})} \\ \frac{\partial G}{\partial r}\Big|_{(r,s)=(\bar{r},\bar{s})} & \frac{\partial G}{\partial s}\Big|_{(r,s)=(\bar{r},\bar{s})} \end{pmatrix}\,. \tag{S5}$$

The assumption of a Turing instability then leads to the following constraints on the reaction kinetics and diffusion parameters:

- For the homogeneous fixed point $(r,s) = (\bar{r},\bar{s})$ to be stable, the real parts of the eigenvalues of the homogeneous stability matrix in Eq. (S5),

$$\lambda_0^{\pm} = \frac{1}{2}\left[r_{11} + s_{22} \pm \left(r_{11}^2 + s_{22}^2 + 4r_{12}s_{21} - 2r_{11}s_{22}\right)^{1/2}\right]\,, \tag{S6}$$

  must be negative. This requirement amounts to the conditions

$$r_{11} + s_{22} < 0\,, \tag{S7}$$

$$r_{11}s_{22} - r_{12}s_{21} > 0\,. \tag{S8}$$

- By definition, the eigenvalues λ of the stability matrix associated with Eqs. (1) and (2) of the main text satisfy an equation of the form

$$\det\left[\begin{pmatrix} A-\lambda & B \\ C & D-\lambda \end{pmatrix}\right] = \lambda^2 - \lambda\,\mathrm{tr}\left[\begin{pmatrix} A & B \\ C & D \end{pmatrix}\right] + \det\left[\begin{pmatrix} A & B \\ C & D \end{pmatrix}\right] \equiv a\lambda^2 + b\lambda + c = 0\,, \tag{S9}$$

which has the solutions

$$\lambda^{\pm} = \frac{1}{2a}\left[-b \pm \left(b^2 - 4ac\right)^{1/2}\right]. \tag{S10}$$

Since $b > 0$ for all wavenumbers[1], for $\mathrm{Re}(\lambda^+)$ to pass through zero we must have $c = 0$ and, hence, the determinant of the stability matrix vanishes for some wavenumbers. Thus, we require that the solutions of

$$\det\left[\begin{pmatrix} A & B \\ C & D \end{pmatrix}\right] \equiv \det\left[\begin{pmatrix} r_{11} - \nu_r(1-\bar{s})(k_x^2+k_y^2) & r_{12} - \nu_r\bar{r}(k_x^2+k_y^2) \\ s_{21} - \nu_s\bar{s}(k_x^2+k_y^2) & s_{22} - \nu_s(1-\bar{r})(k_x^2+k_y^2) \end{pmatrix}\right] \equiv d(k_x^2+k_y^2)^2 - e(k_x^2+k_y^2) + f = 0 \tag{S11}$$

in terms of $(k_x^2 + k_y^2)$ be real. This amounts to demanding $e^2 > 4df$, or

$$\left[\nu_r\bar{r}s_{21} - \nu_r(1-\bar{s})s_{22} + \nu_s\left(\bar{s}r_{12} - (1-\bar{r})r_{11}\right)\right]^2 > 4\nu_r\nu_s(1-\bar{r}-\bar{s})(r_{11}s_{22} - r_{12}s_{21}) > 0\,, \tag{S12}$$

where the last inequality follows from Eq. (S8).

- An estimate of the characteristic scale resulting from the Turing instability can be obtained from the mid-point of the band of unstable modes given by

$$\begin{aligned}(k_x^2+k_y^2)_m &= \frac{1}{2}\left[(k_x^2+k_y^2)_- + (k_x^2+k_y^2)_+\right] \\ &= \frac{\nu_r\left[(1-\bar{s})s_{22} - \bar{r}s_{21}\right] + \nu_s\left[(1-\bar{r})r_{11} - \bar{s}r_{12}\right]}{2\nu_r\nu_s(1-\bar{r}-\bar{s})}\,,\end{aligned} \tag{S13}$$

where $(k_x^2+k_y^2)_-$ and $(k_x^2+k_y^2)_+$ are the zeroes of λ^+ in Eq. (S10). To ensure that the mid-point of the band of unstable modes is real we must have $(k_x^2+k_y^2)_m > 0$, which means that

$$\nu_r\left[(1-\bar{s})s_{22} - \bar{r}s_{21}\right] + \nu_s\left[(1-\bar{r})r_{11} - \bar{s}r_{12}\right] > 0\,. \tag{S14}$$

The characteristic scale is then given by

$$\ell_m = \frac{2\pi}{\sqrt{(k_x^2+k_y^2)_m}}\,. \tag{S15}$$

Solutions of the linearized system associated with the mid-point of the band of unstable modes diverge as e^{vt}, where $v = \mathrm{Re}(\lambda^+)$, which leads to the characteristic time scale $\tau_m = 1/v$.

As discussed in the main text, we require in our Turing model that the receptors are inhibitors and that the scaffolds are activators, which implies $r_{11} < 0$ and $s_{22} > 0$, respectively. But note that, according to the above conditions, we have that $r_{11}s_{22} - r_{12}s_{21} > 0$. This means that r_{12} and s_{21} must have opposite signs. Two generic cases are therefore allowed for the signs of the elements of the homogeneous stability matrix in Eq. (S5):

$$\text{(a)}\ \begin{pmatrix} - & + \\ - & + \end{pmatrix}, \qquad \text{(b)}\ \begin{pmatrix} - & - \\ + & + \end{pmatrix}. \tag{S16}$$

Since scaffold molecules transiently bind, and thereby stabilize, both receptors and scaffolds, we conclude that case (a) applies to our biological system.

[1] This comes about because the homogeneous steady-state is stable and the diffusion terms have a negative overall sign in Fourier space.

S3 Reaction kinetics of synaptic receptor domains

The crucial reactions in our model, encapsulated in Eqs. (1) and (2) of the main text, are $R_b + S \longrightarrow R + S$ for the receptors and $S_b + 2S \longrightarrow 3S$ for the scaffolds, together with the reactions $R \longrightarrow R_b$ and $S \longrightarrow S_b$ corresponding to the endocytosis of receptors and scaffolds. Mathematical expressions describing these reactions are obtained following the mathematical formalism developed in the context of chemical dynamics [4–8]. For instance, the removal of a receptor molecule from the membrane via endocytosis is described by a term $-br$ in F, where b is the rate at which endocytosis proceeds. For reactions which increase the number of molecules at the membrane we account for steric effects by imposing the constraint $0 \leq r + s \leq 1$, leading to a suppression of the relevant reaction rates by a factor $(1 - r - s)$.

The reaction $R_b + S \longrightarrow R + S$, in F, and the reaction $S_b + 2S \longrightarrow 3S$, in G, correspond to the activation of increased receptor concentrations by scaffolds and the self-activation of scaffolds, respectively. In particular, the reaction $R_b + S \longrightarrow R + S$ is the lowest-order reaction in which receptors are stabilized by scaffolds. In terms of the linear stability analysis described in Sec. S2, this activation of receptors by scaffolds amounts to $r_{12} > 0$. Similarly, the reaction $S_b + 2S \longrightarrow 3S$ is the lowest-order reaction which can produce $s_{22} > 0$ in our model. We note, in particular, that the reaction $S_b + S \longrightarrow 2S$ is not sufficient for the self-activation of scaffolds because, together with the constraint that $(r, s) = (\bar{r}, \bar{s})$ is a non-trivial homogeneous fixed point, it violates the condition $0 \leq s \leq 1$ or the condition $s_{22} > 0$.

When simulating Eqs. (1) and (2) of the main text, we allowed, in accordance with experimental observations [3, 9–14], for a variety of chemical reactions between receptors and scaffolds in addition to the essential reactions discussed above:

$$\begin{aligned} F(r,s) &= -b\left(r - \frac{s}{\bar{s}}\frac{1-r-s}{1-\bar{r}-\bar{s}}\bar{r}\right) - m_1\frac{1-r-s}{1-\bar{r}-\bar{s}}(r-\bar{r}) + m_2\frac{1-r-s}{1-\bar{r}-\bar{s}}\frac{r}{\bar{r}}(s-\bar{s}) \\ &= \underbrace{-br}_{R\to R_b}\underbrace{+m_1\frac{1-r-s}{1-\bar{r}-\bar{s}}\bar{r}}_{R_b\to R}\underbrace{+b\frac{1-r-s}{1-\bar{r}-\bar{s}}\frac{\bar{r}}{\bar{s}}s}_{R_b+S\to R+S}\underbrace{-\left(m_1+m_2\frac{\bar{s}}{\bar{r}}\right)\frac{1-r-s}{1-\bar{r}-\bar{s}}r}_{M_b+R\to R_b+M_b}\underbrace{+\frac{m_2}{\bar{r}}\frac{1-r-s}{1-\bar{r}-\bar{s}}rs}_{R_b+R+S\to 2R+S}, \end{aligned} \tag{S17}$$

$$\begin{aligned} G(r,s) &= -\beta\left(s - \frac{1-r-s}{1-\bar{r}-\bar{s}}\bar{s}\right) + \mu\frac{1-r-s}{1-\bar{r}-\bar{s}}\frac{s}{\bar{s}}(s-\bar{s}) \\ &= \underbrace{-\beta s}_{S\to S_b}\underbrace{+\beta\frac{1-r-s}{1-\bar{r}-\bar{s}}\bar{s}}_{S_b\to S}\underbrace{-\mu\frac{1-r-s}{1-\bar{r}-\bar{s}}s}_{M_b+S\to S_b+M_b}\underbrace{+\frac{\mu}{\bar{s}}\frac{1-r-s}{1-\bar{r}-\bar{s}}s^2}_{S_b+2S\to 3S}, \end{aligned} \tag{S18}$$

where we have indicated below each monomial term the corresponding chemical reaction that it describes. The symbol M_b in the above expressions denotes unspecified molecules in the bulk of the cell, which can be receptors or scaffolds. The expressions in Eqs. (S17) and (S18) are arranged so that the reaction terms exhibit a stable homogeneous fixed point at the concentrations $(r, s) = (\bar{r}, \bar{s})$, since $F(\bar{r}, \bar{s}) = 0$ and $G(\bar{r}, \bar{s}) = 0$. It then follows from Eqs. (1) and (2) of the main text that the receptor and scaffold densities are stationary in time if $(r, s) = (\bar{r}, \bar{s})$ everywhere at the membrane. Random perturbations of this fixed point trigger pattern formation via a Turing instability [4–8].

S4 Stable patterns of synaptic receptor domains

To simulate Eqs. (1) and (2) of the main text it is convenient to introduce the dimensionless variables

$$x \to \widetilde{x} = \left(\frac{b}{\nu_r}\right)^{1/2} x\,, \quad y \to \widetilde{y} = \left(\frac{b}{\nu_r}\right)^{1/2} y\,, \quad t \to \widetilde{t} = b\,t\,, \tag{S19}$$

in terms of which Eqs. (1) and (2) of the main text become

$$\frac{\partial r}{\partial \widetilde{t}} = \widetilde{F}(r,s) + \widetilde{\nabla}\left[(1-s)\widetilde{\nabla} r + r\widetilde{\nabla} s\right], \tag{S20}$$

$$\frac{\partial s}{\partial \widetilde{t}} = \widetilde{G}(r,s) + \widetilde{\nu}_s\widetilde{\nabla}\left[(1-r)\widetilde{\nabla} s + s\widetilde{\nabla} r\right], \tag{S21}$$

where $\widetilde{F}(r,s) = \widetilde{F}\left(r,s;\widetilde{m_1},\widetilde{m_2}\right)$ and $\widetilde{G}(r,s) = \widetilde{G}\left(r,s;\widetilde{\beta},\widetilde{\mu}\right)$, with

$$\left(\widetilde{m_1},\widetilde{m_2},\widetilde{\beta},\widetilde{\mu}\right) = \frac{1}{b}\left(m_1,m_2,\beta,\mu\right), \quad \widetilde{\nu_s} = \frac{\nu_s}{\nu_r}, \quad \widetilde{\nabla} = \left(\frac{\partial}{\partial\widetilde{x}},\frac{\partial}{\partial\widetilde{y}}\right). \tag{S22}$$

To restore physical dimensions to the solutions of Eqs. (S20) and (S21), we used typical values of ν_r and b taken from experiments. In particular, a number of experimental studies [3, 11–15] suggest $\nu_r = 10^{-2}\ \mu\text{m}^2\ \text{sec}^{-1}$ as a representative value of the receptor diffusion coefficient. For the rate of receptor endocytosis we used $b = 10^{-1}\ \text{sec}^{-1}$, which roughly corresponds to the upper bound on the range of values of b indicated by experiments [11–13]. Smaller values of b produced patterns similar to those in Fig. 2 of the main text.

Following Sec. S2, the homogeneous stability matrix associated with Eqs. (1) and (2) of the main text, defined in dimensionless form by Eqs. (S20) and (S21) with the reaction kinetics in Eqs. (S17) and (S18), is given by

$$\mathbf{M} = \begin{pmatrix} -(1+\widetilde{m}_1+\frac{\bar{r}}{1-\bar{r}-\bar{s}}) & \widetilde{m}_2+\frac{\bar{r}}{\bar{s}}-\frac{\bar{r}}{1-\bar{r}-\bar{s}} \\ -\widetilde{\beta}\frac{\bar{s}}{1-\bar{r}-\bar{s}} & \widetilde{\mu}-\widetilde{\beta}\frac{1-\bar{r}}{1-\bar{r}-\bar{s}} \end{pmatrix}. \tag{S23}$$

Focusing for the sake of simplicity on the case $\bar{r} = \bar{s} = \epsilon \ll 0.5$, the considerations in Sec. S2 imply that the elements of the stability matrix in Eq. (S23) should satisfy the following constraints.

1. Based on the biophysical properties of receptors and scaffolds, we require the signs of the elements of the homogeneous stability matrix in Eq. (S23) as in case (a) of Eq. (S16). The conditions $r_{11} < 0$ and $s_{21} < 0$ are automatically satisfied, while for $r_{12} > 0$ and $s_{22} > 0$ we need
   - $\widetilde{m}_2 > -1 + \epsilon + O(\epsilon^2)$,
   - $\widetilde{\mu} > \widetilde{\beta} + \epsilon\widetilde{\beta} + O(\epsilon^2)$.
2. The constraints in Eqs. (S7) and (S8) imply
   - $\widetilde{\mu} < \widetilde{\beta} + 1 + \widetilde{m}_1 + \epsilon(\widetilde{\beta}+1) + O(\epsilon^2)$,
   - $\widetilde{\mu} + \frac{\epsilon}{1+\widetilde{m}_1}\widetilde{\mu} + O(\epsilon^2) < \widetilde{\beta} + \epsilon\widetilde{\beta}\left(1+\frac{2+\widetilde{m}_2}{1+\widetilde{m}_1}\right) + O(\epsilon^2)$.
3. Equation (S12) means that
   - $\widetilde{\mu}\left[2\widetilde{\beta} + 2\widetilde{\nu}_s(1+\widetilde{m}_1) - \widetilde{\mu}\right] + O(\epsilon) < \left[\widetilde{\beta} + \widetilde{\nu}_s(1+\widetilde{m}_1)\right]^2 + O(\epsilon)$,
   - $\widetilde{\mu} - \epsilon\widetilde{\mu}\left(1+\frac{\widetilde{m}_1}{1+\widetilde{m}_1}\right) + O(\epsilon^2) < \widetilde{\beta} + \epsilon\widetilde{\beta}\left(1-\frac{2\widetilde{m}_1-\widetilde{m}_2}{1+\widetilde{m}_1}\right) + O(\epsilon^2)$.
4. From Eq. (S13) we find the mid-point of the band of unstable modes

$$(k_x^2+k_y^2)_m = \frac{(1-\bar{s})\widetilde{\mu} - \widetilde{\beta} - \widetilde{\nu}_s\left[1+\bar{r}+(1-\bar{r})\widetilde{m}_1 + \bar{s}\widetilde{m}_2\right]}{2\widetilde{\nu}_s(1-\bar{r}-\bar{s})} \tag{S24}$$

   which, to ensure that the wavenumbers are real, must be greater than zero. According to Eq. (S14) this means that

- $\widetilde{\mu} - \epsilon\widetilde{\mu} > \widetilde{\beta} + \widetilde{\nu}_s(1 + \widetilde{m}_1) + \epsilon\widetilde{\nu}_s(1 + \widetilde{m}_2 - \widetilde{m}_1)$.

The mathematical conditions listed above impose general constraints on the reaction and diffusion properties of receptors and scaffolds in our Turing model.

Equations (S20) and (S21) were simulated on a square lattice with side length 6.3 μm using periodic boundary conditions and a spatial grid with spacing 0.063 μm. We used initial conditions for r and s which were randomly distributed in the interval $[0, 0.01]$, well below our choices $(\bar{r}, \bar{s}) = (0.05, 0.05)$ for the numerical values of $\bar{r}$ and $\bar{s}$. Simulations with a smaller grid spacing and other choices of the maximum amplitude of initial perturbations produced results similar to those presented in Fig. 2 of the main text. Moreover, since Eqs. (S20) and (S21) can generally admit several homogeneous fixed points in addition to $(\bar{r}, \bar{s})$, we checked that, for a given set of dimensionless parameters, r and s indeed approached the fixed point $(\bar{r}, \bar{s})$ for homogeneous initial conditions in the range $(0, 1)$.

For our simulations we used the dimensionless parameter values

$$(\widetilde{m}_1, \widetilde{m}_2, \widetilde{\beta}, \widetilde{\mu}, \widetilde{\nu}_s) = (0.4, 10, 0.5, 0.7, 0.02) \ , \tag{S25}$$

which, upon restoring physical dimensions with the aforementioned values $\nu_r = 10^{-2}\ \mu\text{m}^2\ \text{sec}^{-1}$ and $b = 10^{-1}\ \text{sec}^{-1}$ suggested by experiments [3, 11–15], become

$$\begin{aligned} m_1 &= 4 \times 10^{-2}\,\text{sec}^{-1}\,, \\ m_2 &= 1\,\text{sec}^{-1}\,, \\ \beta &= 5 \times 10^{-2}\,\text{sec}^{-1}\,, \\ \mu &= 7 \times 10^{-2}\,\text{sec}^{-1}\,, \\ \nu_s &= 2 \times 10^{-4}\,\mu\text{m}^2\,\text{sec}^{-1}\,. \end{aligned}$$

As discussed further in the main text and in Sec. S3, the reactions in our Turing model crucial for the activation of receptors and scaffolds are $R_b + S \longrightarrow R + S$ and $S_b + 2S \longrightarrow 3S$, respectively. These reactions are, to lowest order, balanced by the reactions $R \longrightarrow R_b$ and $S \longrightarrow S_b$. This means that, in addition to the values of ν_r and b discussed above, we necessarily need to make choices for the values of the parameters $\widetilde{\beta}$ and $\widetilde{\mu}$ [see Eqs. (S17) and (S18)]. We chose $\widetilde{\beta}$, which corresponds to the rate of scaffold endocytosis, so that $\beta \lessapprox b$ as suggested by experiments [11–13]. The value of $\widetilde{\mu}$ fixes the rate of the reaction $S_b + 2S \longrightarrow 3S$. In the absence of any direct experimental measurements of this rate constant, we chose its value on phenomenological grounds so that $\widetilde{\mu}$ and $\widetilde{\beta}$ took comparable magnitudes, and so that the mathematical conditions listed above were satisfied. Moreover, experiments on scaffold turnover and diffusion suggest [3, 10–15] that $\nu_s \ll \nu_r$ and, hence, $\widetilde{\nu}_s \ll 1$. We chose the particular value $\widetilde{\nu}_s = 0.02$ on phenomenological grounds, so as to be consistent with available experimental data on scaffold diffusion and to satisfy the mathematical constraints mandated by our Turing model. Finally, the parameters $\widetilde{m}_1$ and $\widetilde{m}_2$ are associated with reactions which are not crucial components of our Turing model, but might occur [11–14] between receptors and scaffolds. The particular values of these parameters were chosen to satisfy the mathematical conditions listed above, but our results pertaining to the formation and stability of RSDs did not depend critically on these reactions.

For $b = 10^{-1}\ \text{sec}^{-1}$ the parameter values in Eq. (S25) lead, in units of sec^{-1}, to the reaction rates

$$\begin{aligned} &R \overset{1\times10^{-1}}{\longrightarrow} R_b\,, && S \overset{5\times10^{-2}}{\longrightarrow} S_b\,, \\ &R_b \overset{2\times10^{-4}(1-r-s)}{\longrightarrow} R\,, && S_b \overset{3\times10^{-3}(1-r-s)}{\longrightarrow} S\,, \\ &M_b + R \overset{1(1-r-s)}{\longrightarrow} R_b + M_b\,, && M_b + S \overset{8\times10^{-2}(1-r-s)}{\longrightarrow} S_b + M_b\,, \\ &R_b + S \overset{1\times10^{-1}(1-r-s)}{\longrightarrow} R + S\,, && S_b + 2S \overset{2(1-r-s)}{\longrightarrow} 3S\,, \\ &R_b + R + S \overset{2\times10(1-r-s)}{\longrightarrow} 2R + S\,. \end{aligned}$$

Moreover, with the parameter values in Eq. (S25), Eq. (S15) yields a characteristic length $\ell_m = 1\ \mu$m

and a characteristic time scale $\tau_m = 5$ min. Our estimate of ℓ_m, which approximately corresponds to twice the size of RSDs, agrees closely with the results of the simulations shown in Fig. 2 of the main text. The value of τ_m obtained from the linear stability analysis of our model equations is smaller than the time scale of RSD formation found from our simulations, but larger than the characteristic time scale of 10 sec associated with receptor endocytosis. This might come about because the exponential divergence of solutions associated with the mid-point of the band of unstable modes is only a transient phenomenon, with nonlinear interactions stabilizing the solution in Fig. 2 of the main text. Finally, we note that the parameter values in Eq. (S25), together with the simulations in Fig. 2 of the main text, imply that F is much larger at the center of RSDs than in membrane regions in between domains. This is in agreement with the intuitive expectation following from our Turing model that increased receptor concentrations are stabilized at membrane locations with increased scaffold concentrations. We therefore anticipate that receptors are primarily inserted at RSDs, from where they diffuse on the cell membrane.

S5 Plasticity of synaptic receptor domains

Accounting for local variations of receptor and scaffold diffusion rates in our reaction-diffusion model, we obtain the following modified versions of Eqs. (1) and (2) of the main text:

$$\frac{\partial r}{\partial t} = F(r,s) + \nu_r \nabla \left[(1-s)\nabla(D_r r) + D_r r \nabla s - r^2 \nabla D_r \right] , \tag{S26}$$

$$\frac{\partial s}{\partial t} = G(r,s) + \nu_s \nabla \left[(1-r)\nabla(D_s s) + D_s s \nabla r - s^2 \nabla D_s \right] , \tag{S27}$$

where the functions $D_r = D_r(x,y,t)$ and $D_s = D_s(x,y,t)$ represent spatial and temporal variations in the receptor and scaffold diffusion rates; Eqs. (1) and (2) of the main text are recovered for $D_r(x,y,t) = D_s(x,y,t) = 1$. In addition to the nonlinear corrections to the standard diffusion terms discussed in Sec. S2, Eq. (S26) allows for a current

$$\mathbf{j}_3 = -(1-r-s) r \nabla D_r \, , \tag{S28}$$

with a similar expression for scaffolds in Eq. (S27). This current is in the direction of decreasing D_r and is generated because membrane regions where D_r is reduced represent "sinks" of the diffusive motion of receptors.

The results shown in Fig. 3 of the main text were obtained from simulations of the dimensionless versions of Eqs. (S26) and (S27),

$$\frac{\partial r}{\partial \widetilde{t}} = \widetilde{F}(r,s) + \widetilde{\nabla} \left[(1-s)\widetilde{\nabla}(D_r r) + D_r r \widetilde{\nabla} s - r^2 \widetilde{\nabla} D_r \right] , \tag{S29}$$

$$\frac{\partial s}{\partial \widetilde{t}} = \widetilde{G}(r,s) + \widetilde{\nu}_s \widetilde{\nabla} \left[(1-r)\widetilde{\nabla}(D_s s) + D_s s \widetilde{\nabla} r - s^2 \widetilde{\nabla} D_s \right] , \tag{S30}$$

where we use the same notation as in Sec. S4. We set $D_s(x,y,t) = 1$ and took the function $D_r(x,y,t)$ to be a sum of Gaussians in the spatial variables with a threshold dependence on time:

$$D_r\left(\widetilde{x},\widetilde{y},\widetilde{t}\right) = 1 + \widetilde{A}_r \sum_{i,j,k} \theta\left(\widetilde{t} - \widetilde{t}_i\right) \exp\left[-\frac{(\widetilde{x}-\widetilde{x}_j)^2 + (\widetilde{y}-\widetilde{y}_k)^2}{\widetilde{l}_r} \right] , \tag{S31}$$

where the step function $\theta\left(\widetilde{t}\right)$ is defined by

$$\theta\left(\widetilde{t}\right) = \begin{cases} 1 & \text{if } \widetilde{t} \geq 0, \\ 0 & \text{if } \widetilde{t} < 0. \end{cases} \tag{S32}$$

For all simulations shown in Fig. 3 of the main text, we used the reaction kinetics and values of the model parameters discussed in Secs. S3 and S4, and we set $\widetilde{\ell}_r = 3$ and $\left|\widetilde{A}_r\right| = 1/5$, with periods of presynaptic activity lasting 1 sec, 3 sec, 6 sec, and 10 sec. The qualitative behavior displayed in Fig. 3 of the main text is generic to our model, but the quantitative response of RSDs to presynaptic activity depends on the details of the simulation.

References

[1] J. Meier *et al.*, J. Cell Sci. **113**, 2783 (2000).

[2] M. Rosenberg *et al.*, J. Neurosci. **21**, 5036 (2001).

[3] M. Calamai *et al.*, J. Neurosci. **29**, 7639 (2009).

[4] A. M. Turing, Phil. Trans. R. Soc. B **237**, 37 (1952).

[5] M. C. Cross and P. C. Hohenberg, Rev. Mod. Phys. **65**, 851 (1993).

[6] H. Meinhardt, *Models of biological pattern formation* (Academic Press, London, 1982).

[7] D. Walgraef, *Spatio-Temporal Pattern Formation: With Examples from Physics, Chemistry, and Materials Science* (Springer, New York, 1997).

[8] I. R. Epstein and J. A. Pojman, *An Introduction to Nonlinear Chemical Dynamics: Oscillations, Waves, Patterns, and Chaos* (Oxford University Press, New York, 1998).

[9] S. Okabe *et al.*, Nat. Neurosci. **2**, 804 (1999).

[10] N. W. Gray *et al.*, PLoS Biol. **4**, e370 (2006).

[11] D. Choquet and A. Triller, Nat. Rev. Neurosci. **4**, 251 (2003).

[12] C. G. Specht and A. Triller, BioEssays **30**, 1062 (2008).

[13] A. Triller and D. Choquet, Neuron **59**, 359 (2008).

[14] A. Triller and D. Choquet, Trends Neurosci. **28**, 133 (2005).

[15] J. Meier *et al.*, Nat. Neurosci. **4**, 253 (2001).